ACS OMEGA

http://pubs.acs.org/journal/acsodf

Article

Carbohydrate-Derived Polytriazole Nanoparticles Enhance the Anti-Inflammatory Activity of Cilostazol

M. Verónica Rivas, Daniel Musikant, Rocío Díaz Peña, Daniela Álvarez, Luciana Pelazzo, Ezequiel Rossi, Karina D. Martínez, María I. Errea, Oscar E. Pérez, Oscar Varela, and Adriana A. Kolender*

Cite This: *ACS Omega* 2022, 7, 44631−44642

Read Online

ACCESS | Metrics & More | Article Recommendations | Supporting Information

ABSTRACT: Poly(amide-triazole) and poly(ester-triazole) synthesized from D-galactose as a renewable resource were applied for the synthesis of nanoparticles (NPs) by the emulsification/solvent evaporation method. The NPs were characterized as stable, spherical particles, and none of their components, including the stabilizer poly(vinyl alcohol), were cytotoxic for normal rat kidney cells. These NPs proved to be useful for the efficient encapsulation of cilostazol (CLZ), an antiplatelet and vasodilator drug currently used for the treatment of intermittent claudication, which is associated with undesired side-effects. In this context, the nanoencapsulation of CLZ was expected to improve its therapeutic administration. The carbohydrate-derived polymeric NPs were designed taking into account that the triazole rings of the polymer backbone could have attractive interactions with the tetrazole ring of CLZ. The activity of the nanoencapsulated CLZ was measured using a matrix metalloproteinase model in a lipopolysaccharide-induced inflammation system. Interestingly, the encapsulated drug exhibited enhanced anti-inflammatory activity in comparison with the free drug. The results are very promising since the stable, noncytotoxic NP systems efficiently reduced the inflammation response at low CLZ doses. In summary, the NPs were obtained through an innovative methodology that combines a carbohydrate-derived synthetic polymer, designed to interact with the drug, ease of preparation, adequate biological performance, and environmentally friendly production.

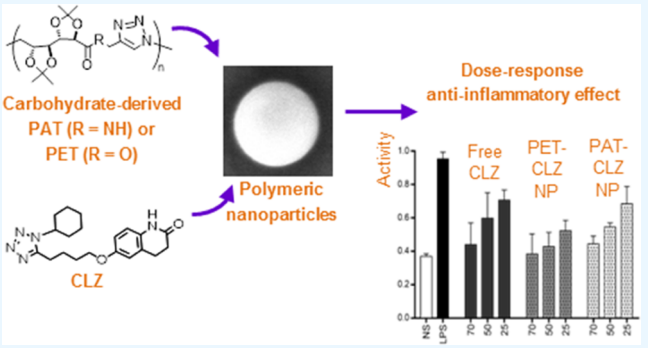

1. INTRODUCTION

Polytriazoles derived from carbohydrates constitute a convenient combination of the abundance, defined stereochemistry, and functionalization of renewable carbohydrates with low toxicity and biological activities of triazole moieties. The use of different protecting strategies on the carbohydrate hydroxyl groups allows the modulation of the hydrophilicity of the repeating units as well as the intra- and intermolecular interactions.[1] Previously, we have described the synthesis and properties of poly(ester-triazole)s[2] (PET) and poly(amide-triazole)s[3] (PAT) derived from D-galactose (Scheme 1). Their precursors were α-azido-ω-alkyne monomers with the secondary hydroxyl groups protected as 1,2-di-*O*-isopropylidene derivatives.

Copper-assisted azide-alkyne cycloaddition (CuAAC) and copper-free (CuFAAC) polymerizations were carried out to study the influence of polymer regiochemistry on properties. The isopropylidene protection in the repeating units led to polymers that were soluble in common organic solvents.[4] PETs were semicrystalline with T_g values of 90−100 °C, while PATs were amorphous materials with higher T_g values (105−135 °C). In both cases, CuFAAC polymerizations gave lower glass-transition temperatures than copper-assisted reactions, consistent with more flexible polymer chains due to loss of regioregularity.

Among the many applications of biomaterials in medicine, the use of nanoparticles (NPs) as drug delivery systems is a relevant issue that merges many disciplines, such as chemistry, physics, medicine, and biology.[5] The discovery of new therapeutic agents has increased the need of NPs as systems able to carry, protect, deliver, and release a specific drug on its target.[6]

Polymeric NPs have been prepared from natural and synthetic polymers for the delivery of drugs, peptides, and nucleotides of low molecular weight.[7] Biodegradable and biocompatible polymers either hydrophobic (poly(lactic acid), poly(glycolic-*co*-lactic acid), poly(ε-caprolactone)) or hydrophilic (chitosan, albumin, alginate, carrageenan, gellan, poly(vinylpyrrolidone)) have been used as a source of NPs.[8−10]

Received: May 12, 2022
Accepted: November 10, 2022
Published: November 30, 2022

Scheme 1. Chemical Structures of Monomers, PET, PAT, and Cilostazol (CLZ)

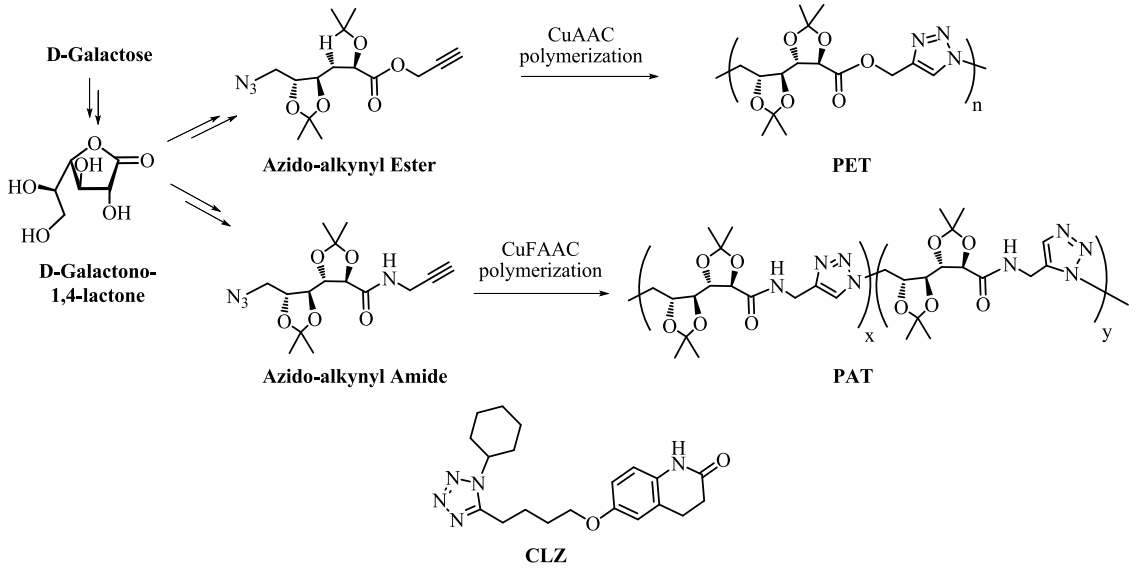

Synthetic polymers usually have a more regular chemical structure than the natural ones and may be tailored according to their intended application. In addition, the drug release could be achieved in periods of days and even weeks, in contrast with natural polymers that have faster release rates, typically associated with easier degradation processes. However, polymerization reactions may include procedures incompatible with sustainability.[11,12] The carbohydrate-derived PATs and PETs may overcome these disadvantages.

The different methods used to obtain polymeric NPs allow control of their physical properties, such as size, morphology, and superficial texture, as well as drug encapsulation efficiency and kinetics of release.[13] The size, shape, and surface of the NPs have great influence on the cell uptake and success of the application.[14] Frequently, the smaller NPs are more easily included in cells.[15] The developments achieved in top-down synthesis of NPs led to more appropriate features, *i.e.*, NPs with improved properties in terms of better size and shape than those obtained from bottom-up strategies.[14] Recently, Bueno-Martinez et al. reported the top-down synthesis of NPs from linear poly(amide-triazole)s derived from D-glucose[16] or D-mannitol[17] for DNA encapsulation and transfection.

The aim of the present work was the application of D-galactose-derived polytriazoles, prepared in our laboratory, in the synthesis of NPs for the encapsulation of CLZ as a proof of concept. This pharmaceutically active ingredient is a vasodilator that inhibits phosphodiesterase III and increases the intracellular concentration of cyclic adenosine monophosphate (AMPc).[18] CLZ is currently applied in the treatment of intermittent claudication, one kind of peripheral arterial disease, but unfortunately it is associated with undesired side-effects.[19] It is poorly soluble in aqueous systems and its bioavailability could be affected by a variable and incomplete absorption.[20] Thus, the nanoencapsulation of CLZ was expected to improve its therapeutic administration.[21] Herein, we describe the synthesis of NPs from galactose-derived PET **3** and PAT **6** (from now on referred as PET and PAT), considering both the difference between the ester/amide bond and the influence of the regioregularity on the polymer backbone. The NPs were employed to encapsulate CLZ, considering that the tetrazole ring of this compound could have attractive interactions with the triazole rings in the polymer backbone. The analysis of the biological activity of the encapsulated drug by means of a metalloproteinase *in vitro* model was carried out as well.

2. EXPERIMENTAL SECTION

2.1. Materials. CLZ kindly supplied by Gador Laboratories (Buenos Aires, Argentina), poly(vinyl alcohol) (PVA, 87−90% hydrolyzed, MW: 30,000−70,000, Sigma-Aldrich), Tween 20 (Merck), Tween 80 (Merck), and Brij-O10 (Croda Inc.) were used as purchased, without further purification. HPLC-grade acetonitrile and HPLC-grade methanol (Sigma-Aldrich) were used for chromatographic determinations.

2.2. Methods. *2.2.1. Synthesis of CuAAC PET and CuFAAC PAT.* PET was synthesized by click CuAAC polymerization of methyl 6-azide-6-deoxy-2,3:4,5-di-*O*-isopropylidene-D-galactonate (**1**) as described previously.[2] Briefly, a solution of monomer **1** (0.350 g, 1.05 mmol) in DMF (3 mL), with 10% CuOAc, was heated under Ar atmosphere at 70 °C for 4 days. The polymer precipitated from the solution during polymerization. It was filtrated, dissolved in dichloromethane, and extracted with NH_4OH (1M) to remove copper salts. After solvent evaporation, PET was obtained as a white solid (90% yield).

PAT was obtained by click CuFAAC polymerization of *N*-propargyl-6-azide-6-deoxy-2,3:4,5-di-*O*-isopropylidene-D-galactonamide (**2**) as described previously.[3] A solution of monomer **2** (0.098 g, 0.29 mmol) in THF (1 mL) was heated under Ar atmosphere at 70 °C for 16 h. After solvent evaporation, the material was dissolved in dichloromethane and precipitated by addition of ethyl ether to afford PAT as a white solid (95% yield).

2.2.2. Preparation of Polymeric NPs by Emulsification/Solvent Evaporation Method. CLZ-loaded NPs (PET-P-CLZ, PAT-P-CLZ) were obtained by adding a solution of the polymer (PET or PAT, 3.75 mg mL^{-1}) and the drug (0.38 mg mL^{-1}) in dichloromethane (1.6 mL) dropwise to a 1% surfactant aqueous solution (Tween 20, Tween 80, Brij-O10, or PVA, 6.4 mL). The mixture was subjected to sonication 3 × 10 min, 240 W (Ultrasonic Homogeneizer 4710 Series, Cole−Parmer Instrument Co., Chicago, Illinois, EEUU 600 Watt

https://doi.org/10.1021/acsomega.2c02969
ACS Omega 2022, 7, 44631−44642

Table 1. Characterization of NPs Obtained from PET and PAT with PVA as Surfactant

			size				
name	polymer	CLZ	DLS diam (nm)	PDI	SEM diam (nm)	pot. ζ	%EE
PET-P-v	PET	no	217 ± 2	0.26 ± 0.04	136 ± 33	−1 ± 3	
PET-P-CLZ	PET	yes	498 ± 21	0.26 ± 0.02	265 ± 40	−1 ± 4	84
PAT-P-v	PAT	no	258 ± 59	0.09 ± 0.02	253 ± 79	−1 ± 4	
PAT-P-CLZ	PAT	yes	234 ± 34	0.10 ± 0.03	178 ± 41	−1 ± 5	80

operating at 40%, equipped with a microtip probe 1/8″ diameter), with the formation of an emulsion, while the system turned translucent. Then, the emulsion was stirred at 37 °C overnight while the organic solvent was evaporated.

Empty NPs (PET-P-v, PAT-P-v) were synthesized in the same way, but the dichloromethane solution contained only the dissolved polymer.

2.2.3. Particle-Size Determinations. The average particle size was measured by dynamic light scattering (DLS) (Zetasizer Nano-Zs, Malvern Instruments, Worcestershire, United Kingdom) with a measurement range of 0.6 nm to 6 μm, provided with a He−Ne laser (633 nm) and a digital correlator (Model ZEN3600). Measurements were carried out at a fixed scattering angle of 173° in disposable polystyrene cuvettes. A multiexponential (CONTIN) approach was applied to obtain size information as intensity size distribution. Through Mie theory, it was converted to size−volume distribution.[22] In all cases, measurements were taken in triplicate for three different batches and the average of these values was reported.

For stability analysis, NP suspensions were stored at 4 °C and DLS measurements were repeated once a week for 4 weeks.

2.2.4. ζ-Potential Measurements. ζ-Potential measurements were performed in a Zetasizer Nano-Zs instrument (Malvern Instruments, Worcestershire, United Kingdom) by evaluation of the electrophoretic mobility of the particles in disposable cells and converted to ζ-potential through Henry's equation. The reported values are the average and standard deviation of three measurements taken in triplicate for three different batches.

2.2.5. Scanning Electron Microscopy (SEM). NP suspensions at 1:200 dilutions in ultrapure water were mounted on aluminum stubs, sputtered with platinum, and analyzed using scanning electron microscopy with a secondary detector on the lens (SEM, Zeiss NTS Supra 40 FEG). Representative SEM images were processed and analyzed with the Fiji Imaging software (Fiji Is Just ImageJ). For NP size determinations, 35−135 particle areas were measured as circles with the Fiji Imaging software. Then, the corresponding diameters were calculated; the means and standard deviations shown in Table 1 were obtained by descriptive statistics.

2.2.6. Nuclear Magnetic Resonance Spectroscopy (NMR). NMR spectra of CLZ and freeze-dried empty or CLZ-loaded NPs (10 mg), dissolved in DMSO-d_6 (0.6 mL), were recorded with a Bruker Avance Neo 500 instrument (^{1}H: 500 MHz) with residual solvent as the internal standard. Assignment of the spectra of CLZ, PVA, PET, and PAT was included in Figures S1−S3.

2.2.7. Fourier Transformed Infrared Spectroscopy (FTIR-ATR). The FTIR spectra (ATR mode) of raw materials, freeze-dried polymeric NPs, and physical mixtures (PhM) of the components (in the same proportions used for the NPs) were recorded in the range 4000−400 cm^{-1} on a Thermo Scientific Nicolet iS50 spectrophotometer.

2.2.8. Differential Scanning Calorimetry (DSC). DSC curves of CLZ, PVA, PET, PAT, freeze-dried NPs, and physical mixtures of the components were obtained with a DSC Q20 TA instrument. Samples of about 2 mg were heated from −10 to 250 °C at a rate of 10 °C min^{-1} (isothermic 5 min) and then cooled at 10 °C min^{-1} to −10 °C (isothermic 5 min). Finally, they were subjected to a second heating cycle at 10 °C min^{-1} to 250 °C (isothermic 5 min).

2.2.9. Encapsulation Efficiency (EE). For the determination of the EE, 1:4 dilutions of the nanosuspensions were centrifuged (Hitachi cp 90nx equipped with a fixed angle rotor P90AT) at 250,000*g* for 2 h when the formation of a pellet was observed. Free CLZ was determined in the supernatant by RP-HPLC/UV[23] using a LC-20AT Prominence Pump, Zorbax Eclipse Plus C18 analytical column (4.6 mm × 150 mm, 5 μm), UV detector (SPD-20AV, Shimadzu Corp., Kyoto, Japan) at 254 nm. The isocratic mobile phase was CH_3CN/H_2O (1:1 v/v) and flow rate was 1.0 mL min^{-1}. CLZ solutions in 1:1 CH_3CN/H_2O were used as external standard in the range 0.5−100 μg mL^{-1}. The EE was calculated using eq 1

$$\%EE = \frac{\text{total drug content} - \text{free drug content}}{\text{total drug content}} \times 100 \quad (1)$$

2.2.10. In Vitro Drug Release Study. The release profile of CLZ was determined by the dialysis diffusion technique.[24] Freshly prepared nanosuspensions of either PET-P-CLZ or PAT-P-CLZ (3.5 mL) were placed into a dialysis bag (Spectra/Por, MWCO 1000) and the system was immersed in PBS buffer (10 mL) with stirring at r.t. Aliquots (1 mL) were withdrawn at predetermined intervals and the volume was replaced with fresh PBS buffer (1 mL). All aliquots were centrifuged (by dilution to a final volume of 10.2 mL) at 250,000*g* for 2 h. Released CLZ was determined by RP-HPLC/UV as described above. Corrections were considered for buffer dilution and for CLZ loss within the aliquots.

2.2.11. Cytotoxicity Study. NP cytotoxicity was tested by the reduction of 3-(4,5-dimethyl-2-thiazolyl)-2,5-diphenyl-2*H*-tetrazolium (MTT) to formazan (deep purple) by mitochondrial dehydrogenases on normal rat kidney cells (NRK)-ATCC CRL 6509.

For evaluation of the biological activities, after the synthesis, the NP suspensions were dialyzed against distilled water (MWCO 6000−8000) for 7 days to remove free CLZ. Then, the suspensions were concentrated and freeze-dried. The solid material was suspended in DMEM (Dulbecco's Modified Eagle Medium, 20 mL) to obtain a 5 mM CLZ stock concentration according to the calculated %EE.

NRK cells were incubated in DMEM supplemented with 10% fetal bovine serum, 100 U mL^{-1} penicillin, and 1 mg mL^{-1}

https://doi.org/10.1021/acsomega.2c02969
ACS Omega 2022, 7, 44631−44642

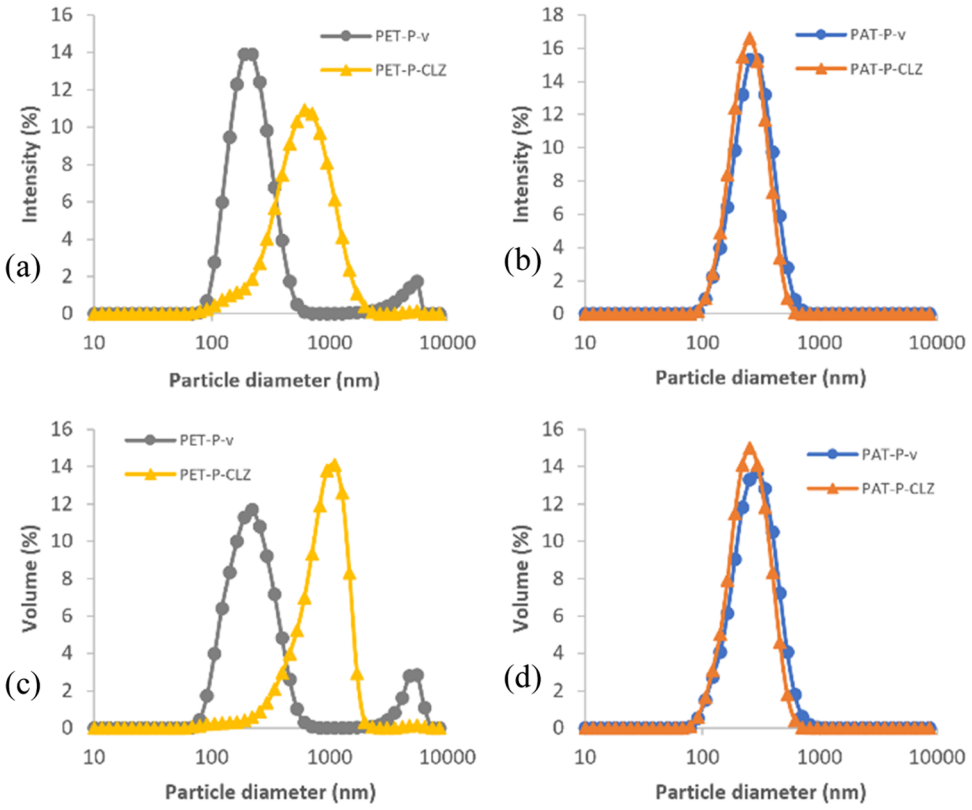

Figure 1. Top: Intensity *vs* particle diameter distribution plot of NPs: (a) PET-P-v and PET-P-CLZ and (b) PAT-P-v and PAT-P-CLZ. Bottom: Volume *vs* particle diameter distribution plot of NPs: (c) PET-P-v and PET-P-CLZ and (d) PAT-P-v and PAT-P-CLZ.

streptomycin. Cells were routinely maintained by serial passages, grown at 37 °C, and in 5% CO_2 atmosphere.

Experiments were carried out on cells incubated in the presence of different concentrations of (a) free CLZ, (b) NPs containing CLZ, (c) empty NPs, or (d) DMEM (control) in 96-well plates for 24 h. For empty NPs, the NP concentration was the same as that of the analogous NPs loaded with CLZ. After treatment, the cells were washed with PBS and incubated with a MTT solution for 3 h. Then, the medium containing MTT was eliminated, DMSO (100 μL/well) was added to dissolve formazan, and absorbance was measured on a microplate reader. The results were analyzed with GraphPad Prism software version 7.00. Half cytotoxic concentration (CC_{50}) was calculated in duplicate, and cells were incubated in quadruplicate for each treatment.

2.2.12. In Vitro Study of CLZ Activity. NRK cells were grown overnight in a 24 multiwell plate. Media was replaced with DMEM-BSA 2% containing lipopolysaccharides from *Escherichia coli* O55:B5 (LPS, Sigma, 1 μg mL^{-1}) with (a) free CLZ, (b) NPs containing CLZ, (c) empty NPs, or (d) DMEM (control). In the first instance, 100 μM free CLZ or the equivalent amount of NPs containing the same CLZ concentration was used. Alternatively, 25, 50, and 75 μM CLZ either free or encapsulated was used for the dose–response experiments. After 24 h, supernatants were collected for gelatinase activity evaluation by gelatin zymography as described previously.[25] Briefly, protein concentration was determined by Bradford (BioRad) and equal amounts of total protein were mixed with loading buffer without a reducing agent and electrophoresed through a 7.5% polyacrylamide gel copolymerized with gelatin 1% (Sigma). An aliquot of supernatant of HT1080 cells stimulated with Phorbol Mirystate Acetate (PMA, 1 μmol L^{-1}) (Sigma) was used as reference for MMP-2 and MMP-9 band positions. Gels were immersed in rinsing buffer (50 mmol L^{-1} Tris–HCl, pH 7.5) with 2.5% Triton X-100 (Panreac) for 1 h, washed 3 times with rinsing buffer, and incubated for 48 h in activation buffer (50 mmol L^{-1} Tris–HCl, 150 mmol L^{-1} NaCl, 10 mmol L^{-1} $CaCl_2$, pH 7.5) at 37 °C. Gels were stained with Coomassie brilliant blue (Sigma). Gelatinolytic activities were detected as pale bands against a dark blue background. Band intensities were quantified using ImageJ software and expressed as Arbitrary Units (AU). During electrophoresis, sodium dodecyl sulfate (SDS) caused latent MMPs to become active and the gelatinolytic activity was distinguished on the basis of their molecular weight.

3. RESULTS AND DISCUSSION

For the NP synthesis, the emulsification/solvent evaporation method was optimized by varying the following parameters: surfactant (Tween 20, Tween 80, Brij-O10, or PVA), concentration of the polymer solution (0.3–4.0 mg mL^{-1}), organic:aqueous phase ratio (1:4 to 1:9), and polymer:CLZ ratio (5:1, 10:1, and 25:1). All of the surfactants employed in this work have been approved by FDA and used in medical applications: PVA,[26] Tween 20, Tween 80, and Brij-O10 (polyoxyethylen (10) oleyl ether).[27]

Since the presence of only 1,4-disubstituted triazole rings or a random mixture of both 1,4- and 1,5-disubstituted moieties along the backbone could affect the physical and chemical properties of the polymers, regioregular PET **3** (synthesized under copper-assisted conditions) and non-regioregular PAT **6** (obtained by copper-free polymerization) were chosen. Both polymers were soluble in common organic solvents and thus

https://doi.org/10.1021/acsomega.2c02969
ACS Omega 2022, 7, 44631–44642

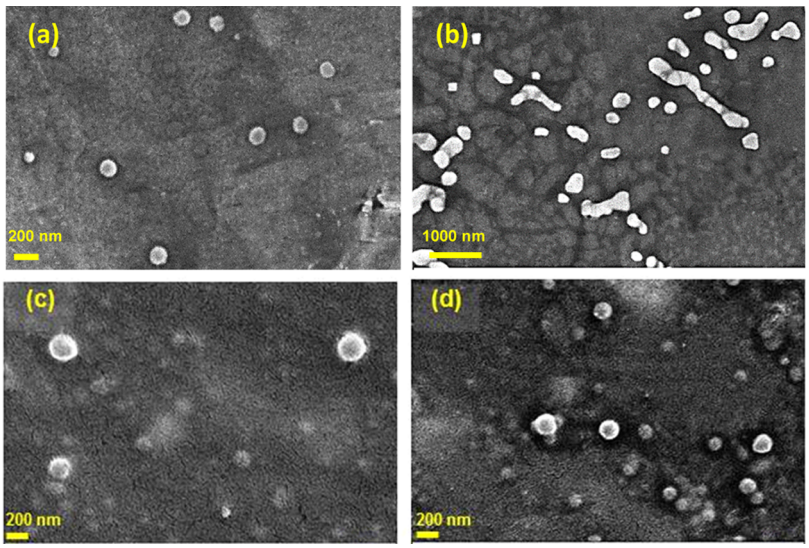

Figure 2. SEM images of NPs: (a) PET-P-v, (b) PET-P-CLZ, (c) PAT-P-v, and (d) PAT-P-CLZ.

the use of the emulsification/solvent evaporation (O/W) method was feasible.

In the first instance, NP formation was assayed using Tween 20 and Tween 80 as surfactants. Unfortunately, they were unable to disperse the organic phase since DLS analysis revealed the presence of several populations of NPs of different sizes. Therefore, both surfactants were considered inappropriate. Preliminary DLS analysis showed average diameters of 200−300 nm for NPs prepared with PVA, and 25 nm for those containing Brij-O10. However, when NPs were prepared in triplicate, the results were not reproducible for Brij-O10. The use of lower polymer concentrations (1 or 0.3 mg mL^{-1}) in the organic phase and higher surfactant concentration (Brij-O10 3%) did not lead to any improvement, so Brij-O10 was excluded as the surfactant. In conclusion, PVA was the surfactant of choice.

3.1. Particle-Size Determinations. The intensity *vs* diameter distribution plot showed a bimodal distribution for empty PET-P-v (Figure 1a). The population of larger size (diameter: 4500 nm) was also observed in the volume distribution graphic with a 10% of the total volume and was assigned to the formation of NP aggregates. The main fraction of PET-P-v (accounting for 90% of the NPs) had diameter values of 217 nm (Table 1). For CLZ-loaded PET NPs (PET-P-CLZ), a unimodal distribution at ∼500 nm was observed. PAT NPs showed unimodal distributions with low polydispersity indexes for both intensity and volume plots. Average particle diameters were 258 and 234 nm for PAT-P-v and PAT-P-CLZ, respectively. It is noteworthy that empty PET NPs have a smaller hydrodynamic radius than the CLZ-loaded NPs, this fact could be understood in terms of a regular PET-PVA arrangement that may be disturbed by the inclusion of CLZ in the system to give a less rigid supramolecular structure. On the other hand, the PAT-PVA system includes amide linkages in a non-regioregular polymer, which can lead to a tighter arrangement due to hydrogen bonding.

The major advantage of particle-size determination by SEM is the direct, high-resolution information about particle size, shape, and texture, but only for a relatively small population of particles on a single image. In consequence, a relevant weakness is that electron microscopy techniques are particle counting methods that produce a number-weighted size distribution that might be biased.[28] In contrast, DLS offers statistically reliable determinations of the mean particle size (hydrodynamic radius) particularly for small particles and low polydispersities. However, DLS has several drawbacks due to the inherent limitation of intensity-biased detection,[29,30] meaning that DLS is very sensitive to the presence of large particles. Thus, small amounts of large aggregates or dust particles can disturb the size determination if the main population is significantly smaller in size.[31] Different methods usually provide different results on particle-size determination and efforts are constantly made to arrive to valid comparisons and precise determinations.[28,31,32] As the use of complementary methods centered on a different basis can overcome these difficulties, scanning electron microscopy has been employed in this work.

Electron microscopy images showed spherical shapes for both PET and PAT systems (Figure 2). At the same time, distortion, collapse, or aggregation were observed in some SEM images of PET-P NPs (Figure 2a,b), in agreement with the register of large particle populations in DLS experiments. Average NP diameters were calculated from the images (only isolated NPs were considered for SEM statistics, Table 1). It is worth to mention that our hydrophilic polymer-stabilized NPs seem to display, according to DLS measurements, a surface corona of hydrated polymer chains. The smaller NP diameters observed in SEM experiments, compared to the hydrodynamic diameters determined by DLS, were attributed to the fact that in the microscopies, the samples were exposed to high vacuum, which would induce a collapse of the hydrated polymer corona.[32]

3.2. ζ-Potential Measurements. The ζ potential of NPs was measured and values near to zero were obtained in all cases (Table 1). This result was expected, since the polymers involved in the formulations have only neutral functionalities in their structures (protected or free hydroxyl, triazole, ester, or amide groups). Nevertheless, NPs showed to be stable on time (see Section 3.7).

3.3. NMR Spectroscopy. ^{1}H NMR spectra of the freeze-dried PET-P and PAT-P NPs have been recorded in DMSO-d_6 to confirm the presence of CLZ (Figures 3 and S1−S3). The lactam-NH (9.89 ppm) and aromatic ether (6.78−6.71 ppm) protons of free CLZ (3c) appeared in a clean region of the

https://doi.org/10.1021/acsomega.2c02969
ACS Omega 2022, 7, 44631−44642

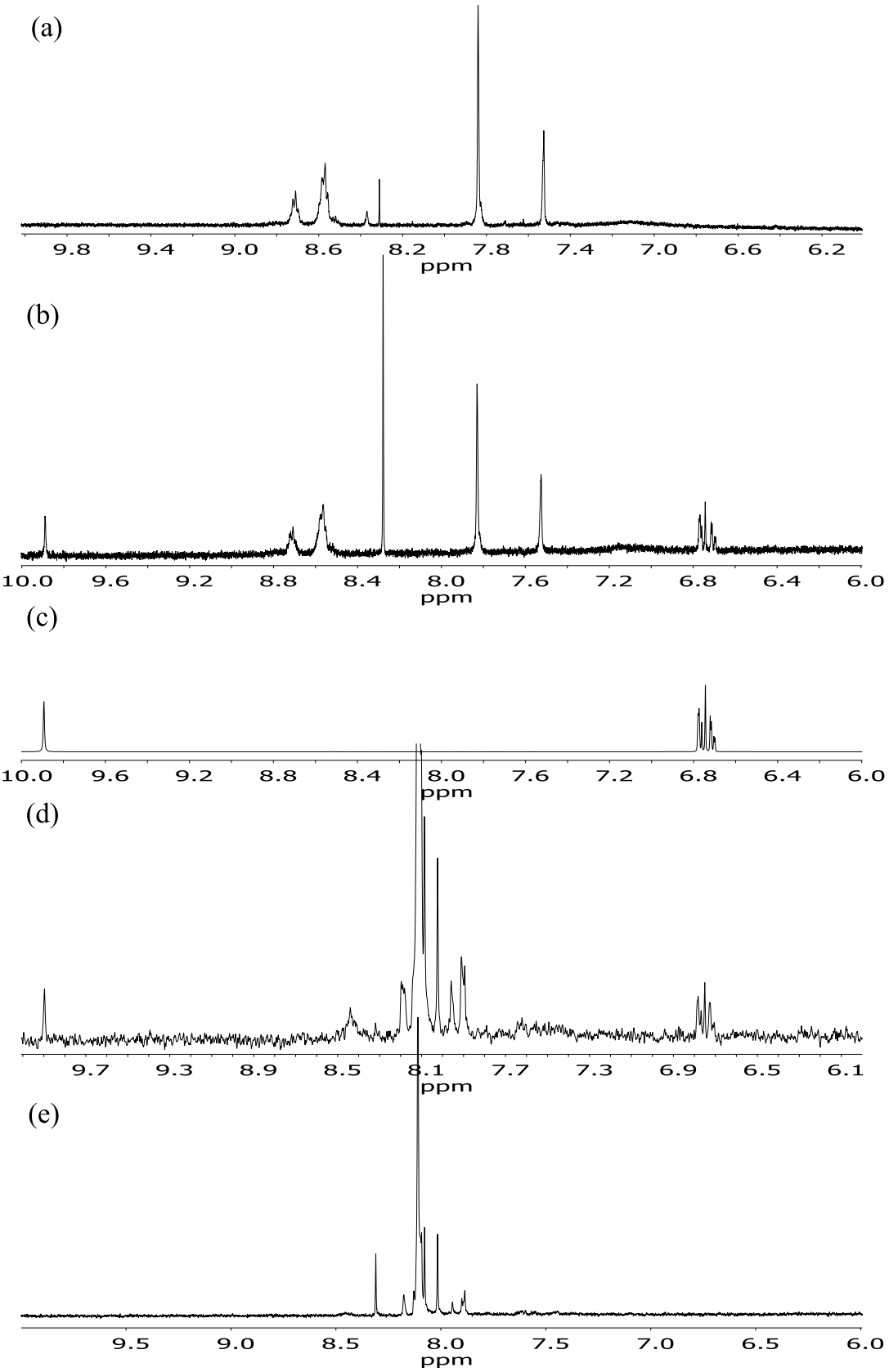

Figure 3. Aromatic and NH region of ^{1}H NMR spectra (500 MHz, DMSO-d_6) of (a) PAT-P-CLZ, (b) PAT-P-v, (c) CLZ, (d) PET-P-CLZ, and (e) PET-P-v.

spectra and remained unchanged in the dissolved NP systems.
For PET-P-CLZ (3e) and PAT-P-CLZ (3a), the PET/CLZ

https://doi.org/10.1021/acsomega.2c02969
ACS Omega 2022, 7, 44631−44642

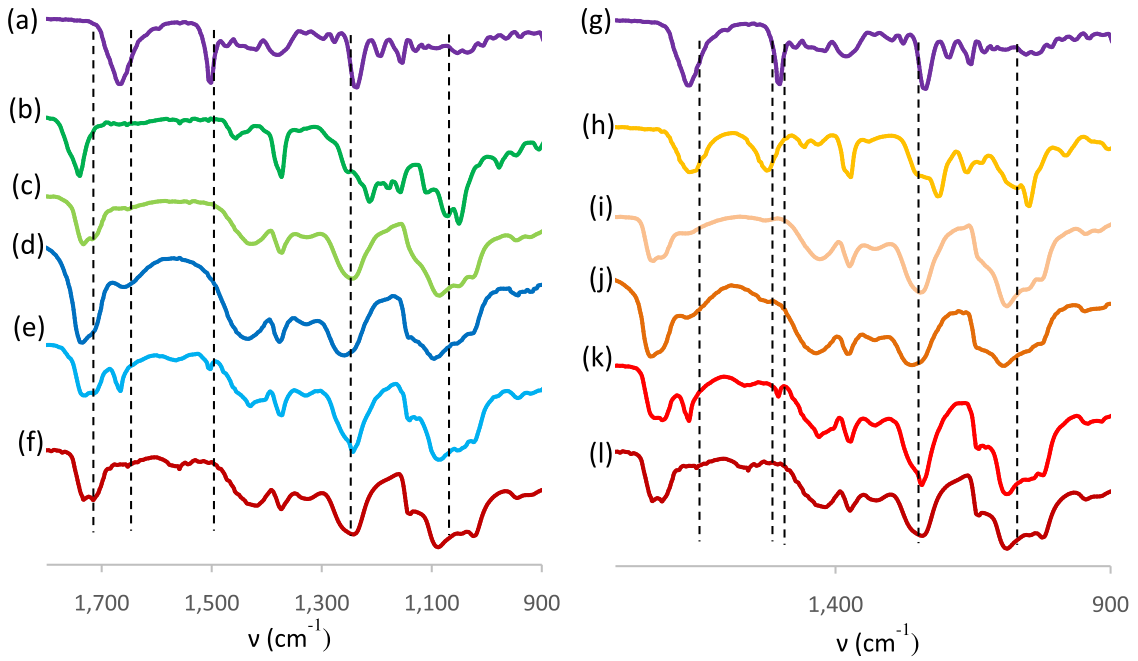

Figure 4. FTIR-ATR spectra of (a) CLZ, (b) PET, (c) PET-P-v NPs, (d) PET-P-CLZ NPs, (e) physical mixture PET + P + CLZ, (f) PVA, (g) CLZ, (h) PAT, (i) PAT-P-v NPs, (j) PAT-P-CLZ NPs, (k) physical mixture PAT + P + CLZ, and (l) PVA.

and PAT/CLZ ratios were 1:0.07 and 1:0.09, respectively, in agreement with those expected according to the NP composition and the EE (Section 3.6).

In addition, the ^{1}H NMR spectrum of PAT-P-v NPs (3e) showed a main peak at 7.84 and a minor one at 7.53 ppm, respectively, assigned to 1,4- and 1,5-disubstituted triazole CH.[3] In the presence of CLZ, the main signal became less intense and the weak one at lower field (8.31 ppm) appeared more intense. The significant downfield shift for this signal suggested that, in spite of the presence of a competitive solvent as DMSO, the triazole CH was also involved in a hydrogen bonding interaction with CLZ. Moreover, neither the proton signals of the dihydroquinolinone ring (NH, aromatic) of CLZ nor the amide-NH of PAT were affected, suggesting that the tetrazole ring of the drug was involved in the interaction with the triazole ring of PAT in DMSO solution.

3.4. Infrared Spectroscopy. FTIR spectra have been recorded for each component of the NPs (amorphous CLZ, PET, PAT, PVA, Figure S4a−c,j), a physical mixture of these components in the same ratio as present in the formulations (Figure S4f,i), and for the four freeze-dried NP samples (PET-P-v, PET-P-CLZ, PAT-P-v, PAT-P-CLZ, Figure S4d,e,g,h). The spectrum of pure amorphous CLZ showed absorption bands assigned to amide N−H (stretching, 3210 cm^{-1}), aromatic C−H (stretching, 3059 cm^{-1}), CH_2 (asymmetric and symmetric stretching, 2934 and 2858 cm^{-1}), amide C═O (stretching 1668 cm^{-1}), C═C stretching and N−H bending (overlapped at 1503 cm^{-1}), aryl alkyl ether C−O (1236 and 1038 cm^{-1}, asymmetric and symmetric stretching, respectively)[21] overlapped with −N═N−N− (1236 cm^{-1}), and tetrazole ring (1151 cm^{-1}).[33,34]

The main signals found in the FTIR spectrum of PVA were attributed to hydroxyl and carbonyl groups, namely, O−H stretching associated to inter- and intramolecular hydrogen bonds at 3292 cm^{-1} (br), C−H from alkyl groups at 2942 and 2910 cm^{-1}, C═O stretching vibrations at 1733 and 1716 cm^{-1} (derived from residual acetylation of the polymer), C−H_2 bending at 1418 cm^{-1}, and C−O stretching at 1089 cm^{-1}.[35]

In a more detailed analysis of the spectra in the 1800−900 cm^{-1} diagnostic region (Figure 4), both PET NP (PET-P-v and PET-P-CLZ) spectra revealed a weak signal corresponding to the C═O stretching from PET, since the signal at 1733 cm^{-1} was slightly increased in comparison to the spectrum of pure PVA. Stretching vibration corresponding to C−O from PET was also observed (1050 cm^{-1}).

In the case of PAT NPs (PAT-P-v and PAT-P-CLZ), absorptions corresponding to the amide moiety appeared as a broad signal at 1670 cm^{-1} (amide I band) and 1526 cm^{-1} (amide II band) in addition to C−O bending from the sugar residue at 1051 cm^{-1}.

In the spectra of all NPs, either from PET or PAT, signals coming from PVA were clearly observed. However, bands associated to CLZ were weak, probably due to the low amount of CLZ present in the NP formulation. Therefore, physical mixtures of the four components in the same ratios present in the NPs were prepared (by thoroughly mixing the components in a mortar) and the FTIR spectra were recorded (Figures S4 and 4e,k). For the mixtures from PET or PAT, the main absorptions of CLZ have been detected (C═O at 1666 cm^{-1}, C═C stretching and amide II band at 1504 cm^{-1}, and C−O overlapped with −N═N−N− at 1236 cm^{-1}). More careful observation of the spectra of CLZ-loaded NPs showed a more intense absorption at 1660 cm^{-1}, together with an evident broadening of the band centered at 1245 cm^{-1} due to an increase in the absorption at 1264 cm^{-1} (Figure 4d for PAT-P-CLZ and Figure 4j for PET-P-CLZ). Both signals were attributed to the CLZ encapsulated in the NPs. Furthermore, the up-shift of the signals from 1236 to 1264 cm^{-1}, observed only in the CLZ-loaded NPs, was consistent with interactions of the tetrazole ring of CLZ, proposed after NMR analysis.[33]

3.5. Differential Scanning Calorimetry. DSC studies were carried out to analyze changes in the thermal behavior of the NP components. The second-heating DSC curves

https://doi.org/10.1021/acsomega.2c02969
ACS Omega 2022, 7, 44631−44642

performed for pure CLZ, PVA, PET, PAT, the physical mixtures, and the freeze-dried NPs have been recorded (Figure S5). Thermogram of pure amorphous CLZ showed an exothermic event associated to crystallization at 74 °C followed by melting at 160 °C, in the first heating curve.[21] The second heating cycle revealed only a T_g at 35 °C. However, this glass-transition temperature was not detected either in the NPs or in the physical mixture curves (see below). Two events were evidenced in the PVA thermogram. The first one corresponded to a glass transition (T_g = 70 °C) followed by an endothermic process assigned to a relaxation of the material stress. The second event was a broad endothermal transition corresponding to PVA melting (T_m 173 °C).[36] As expected, events associated to PVA transitions were visible in all of the NP and physical mixture curves. In PET-P-v NPs, the glass transition corresponding to PET (T_g = 95 °C) was observed at 97 °C, while the PAT T_g (expected at 116 °C) was not detected in the thermograms of PAT NPs. Changes in the thermal behavior of the NP components could indicate amorphization of CLZ together with intermolecular interactions in the solid state, in agreement with the absorption shifts in the FTIR spectra of the NPs. The loss of crystallinity of CLZ could modulate its diffusion through the polymeric shell, resulting in an enhanced and sustained release from the nanocarriers.[21]

3.6. Encapsulation Efficiency (EE). For drug loading EE, diluted nanosuspensions were centrifuged until pellet formation was observed. Free CLZ was measured in the supernatant by RP-HPLC/UV. A calibration curve was obtained with CLZ solutions and EE was calculated using eq 1. For PET-P-CLZ and PAT-P-CLZ NPs, the EE was estimated as 84 and 80%, respectively. These results were consistent with the NP composition determined by ^{1}H NMR analysis.

3.7. Stability Study. The NP colloidal suspensions preserved the same visual aspect without precipitation or color change, while the average particle size did not show any significant change through periods of 30 days, indicating stability. The stability may not seem to agree with the ζ potential value, which was near to zero. However, the ζ potential is related to electrostatic repulsive forces and does not provide any insight on attractive van der Waals forces.[37] Therefore, the PET and PAT NPs constituted examples of the use of PVA as an effective stabilizer for systems of low ζ potential.

3.8. *In Vitro* Drug Release Study. The CLZ release from NPs was determined (Figure 5) using a dialysis bag immersed in PBS buffer, the same media employed to evaluate the biological activity *in vitro*. Initial encapsulation efficiencies were in agreement with the results mentioned above, *i.e.*, 83.4 and 76.0% for PET and PAT nanoformulations, respectively. After 24 h, the cumulative release increased to 57 (PET-P-CLZ) and 75% (PAT-P-CLZ). For PAT NPs, the release reached a plateau after 48 h with 84%, while after 4 days, the CLZ was still increasing for PET NPs. Therefore, the nanoencapsulation of CLZ effectively slowed the drug release in both formulations, which may prolong its therapeutic effect.

The supramolecular arrangements of the NPs involve a hydrophilic surfactant/stabilizer (PVA) and a highly functionalized hydrophobic polymer (PAT/PET), which can be regioregular (PET) or not (PAT). The CLZ is included in this arrangement and it seems to display attractive interactions between its tetrazole group and the triazole of the polymer.

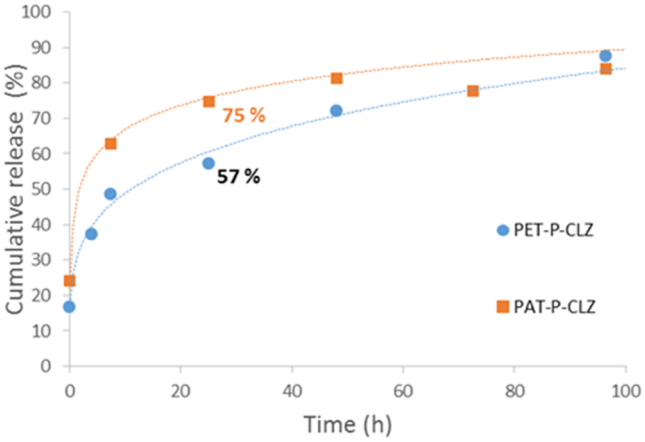

Figure 5. Cumulative release of CLZ *vs* time.

These interactions, of diverse nature (π stacking, dipole−dipole, or H-bonding) according to the chemical structure of the polymers, were experimentally supported by both NMR (in solution) and IR (in solid state). Thus, PET is a regioregular polymer carrying ester groups that can only act as H-bond acceptors; while PAT is non-regioregular and the amide function can behave as donor and acceptor of H-bonding. The increase in the size of PET NPs upon inclusion of CLZ could arise from an alteration of the ordered disposition of the regioregular PET chains (PET is obtained in a semicrystalline state with T_m 204 °C in the first heating cycle of DSC).[2] The disruption of the ordered arrangement to accommodate CLZ gives rise to an increase of the diameter. In contrast, PAT NPs maintain their size while including the CLZ in the formulation. This could be the consequence of the formation of an intricate network through H-bonding of the PAT amide groups. This arrangement is expected not to be perturbed by the inclusion of CLZ. In addition, non-regioregular PAT chains (PAT is obtained as an amorphous material)[3] would allow conformational flexibility in a dynamic system that can either accommodate or expel the drug to reestablish the ordered arrangement. Therefore, CLZ could be released faster from PAT NPs, as experimentally observed.

In spite of this discussion, the final and more relevant result was that CLZ-loaded PET NPs showed a higher anti-inflammatory activity in the more complex cell environment, as discussed below.

3.9. Cytotoxicity Assays. Cytotoxicity assays were carried out to determine if any of the components included in the NP systems could be deleterious for cell viability. Thus, experiments were conducted in the presence of free CLZ, CLZ-loaded NPs, and empty NPs at the same concentration as those carrying the drug. The half cytotoxic concentration (CC_{50}) was calculated (Figure S4). For empty NPs, the CC_{50} values were much higher than free CLZ, indicating that neither the polymer nor the PVA were toxic. The CC_{50} for free CLZ was 119.5 μM (Table 2), while it was higher for PAT-P-CLZ NPs (213.7 μM). The PET-P-CLZ NPs were less cytotoxic than free CLZ as well (135.4 μM). These facts supported the initial hypothesis that nanoencapsulated CLZ was less toxic. The subsequent step was the *in vitro* evaluation of the activity of the nanoencapsulated CLZ.

3.10. *In Vitro* Study of CLZ Activity. Matrix metalloproteinases (MMPs) are a well characterized proteolytic Zn^{+2}-dependent enzyme family associated with several bio-

https://doi.org/10.1021/acsomega.2c02969
ACS Omega 2022, 7, 44631−44642

Table 2. CC_{50} for Free CLZ and NPs Synthesized by the Emulsification/Evaporation Method

	free CLZ	PAT-P-v	PAT-P-CLZ	PET-P-v	PET-P-CLZ
CC_{50} (μM)	120	348	135[a]	>500.0	214[a]
error (μM)	5	29	26		15

[a]For empty NPs, the CC_{50} was determined using the same NP concentration of those NPs loaded with CLZ.

logical processes. Both physiological and pathological roles have been described for MMPs.[38] Specifically, two members of the family, MMP-2 and MMP-9, possess enzymatic activity on collagen type IV (a component of basal membranes). Hence, its activity is essential for crossing through the endothelium of inflammatory cells. Cleavage of matrix elements by MMP-2 and MMP-9 leads to release of growth factors, hormones, cytokines, and chemoattractants. Therefore, its relevance in neoplastic processes, infectious diseases, and its key role in chronic inflammatory processes have been highlighted.[38] Previous studies have shown that CLZ prevents MMP-9 tissue inflammation in both *in vivo* and *in vitro* models.[39,40] In this work, a cellular model has been used to measure the effect of NPs containing CLZ on MMP-2 and MMP-9 activity in culture supernatants. Supernatants of cells incubated with bacterial lipopolysaccharide (LPS), as inflammatory stimulus, showed a significant induction of MMP-9 activity compared to nonstimulated cells (NS, control, Figure 6a). Cotreatment with LPS and free CLZ (100 μM) was able to modulate the MMP-9 activity induction (Free CLZ in Figure 6a) and the same effect was observed when cells were treated with LPS and CLZ-loaded NPs (PET-P-CLZ and PAT-P-CLZ, Figure 6a). The MMP-2 activity did not reveal any difference with these treatments, probably because MMP-2 and MMP-9 have different regulations at several levels.[38] It is noteworthy that empty NPs (PET-P-v and PAT-P-v, Figure 6a) had a regulation effect on MMP-9 at the same level than free CLZ, and it was enhanced when CLZ was nanoencapsulated. This indicated that the NPs themselves had regulatory activity on MMP-9, which may be attributed to the presence of triazole moieties combined with isopropylidene-protected repeating units. These polymers would enhance the permeation through the cell membranes, leading to inhibitory activity.[41]

It is noteworthy as well that NRK cells were subjected to LPS stimulation in the presence of CLZ-containing NPs for 24 h and that the drug release was close to 57 and 75% for PET-P-CLZ and PAT-P-CLZ, respectively, in this time lapse (see Figure 5). It means that even though the nominal concentration of CLZ in the NPs was the same as the free CLZ, the actual concentration released to the media was lower for the samples treated with encapsulated CLZ. Nevertheless, the drug activity was equal or better than the free drug.

Once determined that MMP-9 was a valid model for the evaluation of CLZ activity *in vitro*, a dose−response experiment was performed. Thus, 25, 50, and 75 μM doses of free CLZ and NPs containing the same nominal concentration of the drug (Figure 6b) were evaluated and compared with nonstimulated (NS) or LPS-stimulated (LPS) NRK cells. A significant regulation of MMP-9 at least up to 25 μM was observed for PAT-P-CLZ and even better for PET-P-CLZ, in spite of the release profile described in PBS. The higher anti-inflammatory activity observed for PET-P-CLZ NPs could be explained considering that these NPs have higher diameters (Table 1), which implies a less tight arrangement of the

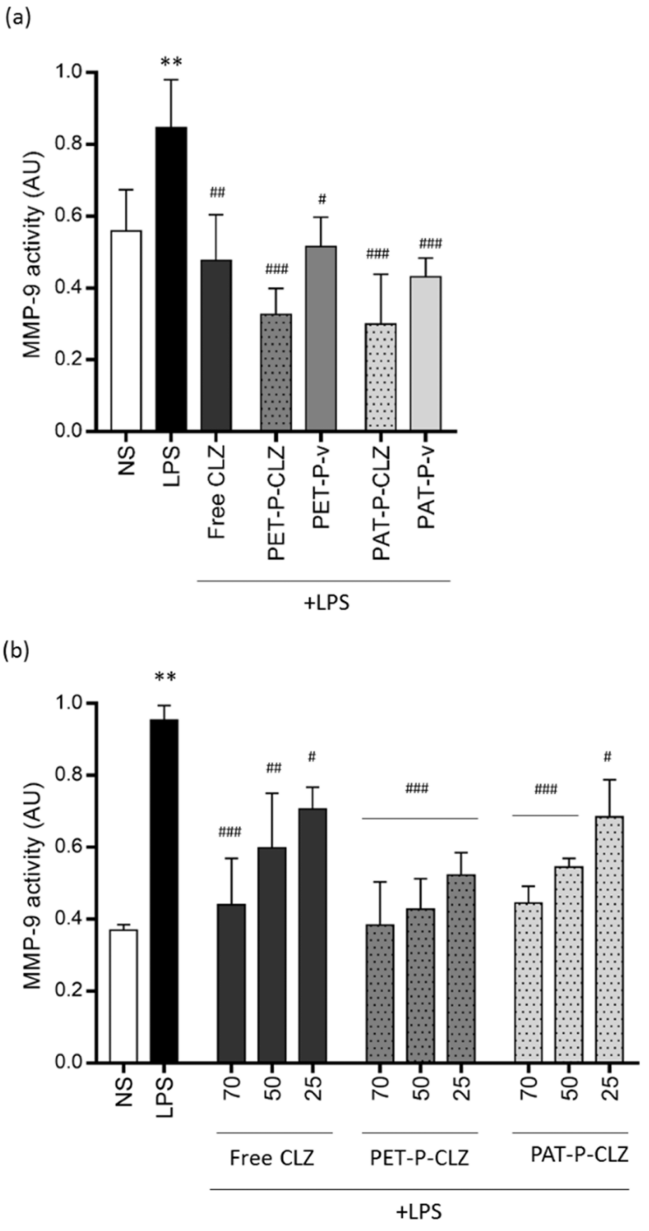

Figure 6. *In vitro* CLZ activity. MMP-9 gelatinase activity was determined by zymography in supernatants of NRK cells after 24 h of the indicated treatments (a) at 100 μM CLZ or (b) in a dose−response experiment at 70, 50, and 25 μM CLZ in the presence of LPS stimulus or in nonstimulated cells (NS). $^{**}p < 0.01$ *vs* NS; $\#p < 0.05$; $\#\#p < 0.01$; $\#\#\#p < 0.001$ *vs* LPS.

polymeric chains. In addition, ester bonds are more easily hydrolyzed than amide linkages and polyesters such as poly(ε-caprolactone), polyhydroxyalkanoates, poly(lactic acid), and poly(glycolic acid) are well known examples of biodegradable polymers.[42] Therefore, looser PET-P-CLZ NPs immersed in a cell culture would be more susceptible to hydrolysis than smaller and less reactive PAT-P-CLZ NPs. As a result, CLZ would be released and would exert its anti-inflammatory activity more efficiently when included in PET NPs.

4. CONCLUSIONS

Polymeric NPs have been successfully prepared from D-galactose-derived PET or PAT polytriazoles. Synthetically modified carbohydrates have been employed as monomer

https://doi.org/10.1021/acsomega.2c02969
ACS Omega 2022, 7, 44631−44642

precursors of PET or PAT, in view of the intensive use of carbohydrate derivatives for the development of biologically active formulations.[43] Structural differences in the backbone of these polymers (inclusion of ester in PET or amide functions in PAT, and the regioregularity in PET or non-regiooregularity in PAT) affected the formation and properties of the resulting NPs. The NPs, prepared by the emulsification/solvent evaporation method using PVA as the stabilizer, were convenient for the efficient encapsulation of CLZ. Both PET and PAT NPs were characterized by their morphology, size, and stability by DLS and SEM. The NPs were spherical with hydrodynamic diameters in the range of 217−258 nm for PAT-P-v, PAT-P-CLZ, and PET-P-v, while PET-P-CLZ showed higher values in solution (∼500 nm). PVA proved to be a good stabilizer for these systems, in spite of their low ζ potentials. NMR and IR spectroscopies confirmed the presence of CLZ within the NPs and supplied evidences of attractive interactions between triazole moieties in polytriazoles and tetrazole rings in CLZ.

Regarding the biological activity, none of the components of the chosen NPs were cytotoxic for NRK cells. In particular, polytriazoles derived from D-galactose exhibited some beneficial properties that enhanced cell growth even in the presence of CLZ. The CLZ activity was measured *in vitro* by means of a MMP-9 model in a LPS-induced inflammation system. Both PAT and PET NPs were able to modulate the MMP-9 activity in an inflammatory model, and such an activity was enhanced when CLZ-loaded NPs were used. Higher anti-inflammatory activity was registered for PET-P-CLZ even at a 25 μM dose. This fact could be related to a less tight arrangement of more hydrolysable polymers in the NPs that would enhance the CLZ release when in a cell culture medium.

The results obtained for cytotoxicity, drug release, and modulation of the inflammatory stimulus are very promising since a stable, noncytotoxic NP system efficiently modulated the inflammation response at lower CLZ doses. PAT and PET have been synthesized from a simple monosaccharide, regarding many principles of Green Chemistry, and the NPs introduced herein constitute an innovative system combining interesting biological performance and extended possibilities for an approved drug. As CLZ has been investigated for the treatment of several pathologies, such as Alzheimer's disease,[44] alcoholic liver disease,[45] and acute ischemic stroke,[46] further experiments will be carried out for the evaluation of our NPs as nanocarriers of CLZ for these and other diseases related to inflammatory processes.

■ ASSOCIATED CONTENT

Supporting Information

The Supporting Information is available free of charge at https://pubs.acs.org/doi/10.1021/acsomega.2c02969.

^{1}H NMR spectra of CLZ (Figure S1); ^{1}H NMR spectra of PET-P-CLZ (Figure S2); ^{1}H NMR spectra of PAT-P-CLZ (Figure S3); FTIR-ATR spectra in the range of 400−4000 cm^{-1} (Figure S4); DSC second-heating thermograms (Figure S5); and MTT absorbance *vs* log CLZ concentration for free CLZ and NPs (Figure S6) (PDF)

■ AUTHOR INFORMATION

Corresponding Author

Adriana A. Kolender − *Universidad de Buenos Aires (UBA), Facultad de Ciencias Exactas y Naturales, C1428EHA Buenos Aires, Argentina; Consejo Nacional de Investigaciones Científicas y Técnicas (CONICET)-UBA, Centro de Investigación en Hidratos de Carbono (CIHIDECAR), C1428EHA Buenos Aires, Argentina;* orcid.org/0000-0001-9933-6556; Email: adrianak@qo.fcen.uba.ar

Authors

M. Verónica Rivas − *Universidad de Buenos Aires (UBA), Facultad de Ciencias Exactas y Naturales, C1428EHA Buenos Aires, Argentina; Consejo Nacional de Investigaciones Científicas y Técnicas (CONICET)-UBA, Centro de Investigación en Hidratos de Carbono (CIHIDECAR), C1428EHA Buenos Aires, Argentina*

Daniel Musikant − *Universidad de Buenos Aires (UBA), Facultad de Ciencias Exactas y Naturales, C1428EHA Buenos Aires, Argentina; Consejo Nacional de Investigaciones Científicas y Técnicas (CONICET)-UBA, Instituto de Química Biológica de la Facultad de Ciencias Exactas y Naturales (IQUIBICEN), C1428EHA Buenos Aires, Argentina*

Rocío Díaz Peña − *Universidad de Buenos Aires (UBA), Facultad de Ciencias Exactas y Naturales, C1428EHA Buenos Aires, Argentina; Consejo Nacional de Investigaciones Científicas y Técnicas (CONICET)-UBA, Instituto de Química Biológica de la Facultad de Ciencias Exactas y Naturales (IQUIBICEN), C1428EHA Buenos Aires, Argentina*

Daniela Álvarez − *Universidad de Buenos Aires (UBA), Facultad de Ciencias Exactas y Naturales, C1428EHA Buenos Aires, Argentina; Consejo Nacional de Investigaciones Científicas y Técnicas (CONICET)-UBA, Instituto de Química Biológica de la Facultad de Ciencias Exactas y Naturales (IQUIBICEN), C1428EHA Buenos Aires, Argentina*

Luciana Pelazzo − *Universidad de Buenos Aires (UBA), Facultad de Ciencias Exactas y Naturales, C1428EHA Buenos Aires, Argentina; Consejo Nacional de Investigaciones Científicas y Técnicas (CONICET)-UBA, Centro de Investigación en Hidratos de Carbono (CIHIDECAR), C1428EHA Buenos Aires, Argentina;* orcid.org/0000-0002-9925-4080

Ezequiel Rossi − *Instituto Tecnológico de Buenos Aires (ITBA), C1437FBG Buenos Aires, Argentina*

Karina D. Martínez − *Facultad de Arquitectura Diseño y Urbanismo, Universidad de Buenos Aires (UBA), C1428EHA Buenos Aires, Argentina; Consejo Nacional de Investigaciones Científicas y Técnicas (CONICET)-UBA, Instituto de Tecnología en Polímeros y Nanotecnología (ITPN), C1428EHA Buenos Aires, Argentina;* orcid.org/0000-0002-5208-6067

María I. Errea − *Instituto Tecnológico de Buenos Aires (ITBA), C1437FBG Buenos Aires, Argentina*

Oscar E. Pérez − *Universidad de Buenos Aires (UBA), Facultad de Ciencias Exactas y Naturales, C1428EHA Buenos Aires, Argentina; Consejo Nacional de Investigaciones Científicas y Técnicas (CONICET)-UBA, Instituto de Química Biológica de la Facultad de Ciencias Exactas y Naturales (IQUIBICEN), C1428EHA Buenos Aires, Argentina*

https://doi.org/10.1021/acsomega.2c02969
ACS Omega 2022, 7, 44631−44642

Oscar Varela − *Universidad de Buenos Aires (UBA), Facultad de Ciencias Exactas y Naturales, C1428EHA Buenos Aires, Argentina; Consejo Nacional de Investigaciones Científicas y Técnicas (CONICET)-UBA, Centro de Investigación en Hidratos de Carbono (CIHIDECAR), C1428EHA Buenos Aires, Argentina;* orcid.org/0000-0002-0952-608X

Complete contact information is available at: https://pubs.acs.org/10.1021/acsomega.2c02969

Author Contributions

The project was designed and supervised by A.K. Polymer synthesis, NP characterization, and manuscript draft were performed by M.V.R. Biological activity and manuscript draft were performed by D.M. NP characterization and release studies were performed by V.R., R.D.P., D.A., L.P., and O.E.P. NP characterization by DLS was performed by E.R., K.M., and M.I.E. Part of the experimental work was supervised by O.V. who also revised the manuscript.

Notes

The authors declare no competing financial interest.

■ ACKNOWLEDGMENTS

This work was supported by the National Research Council of Argentina (CONICET, Project PIP 11220150100443CO) and the University of Buenos Aires (UBA, Project 20020170100403BA). M.V.R., R.D.P., D.A., and L.P. are fellows from CONICET. D.M., K.D.M., M.I.E., O.E.P., O.V., and A.A.K. are research members from CONICET. The authors are grateful to Dr. Constanza Mangone (Gador Laboratories) for kindly supplying the CLZ samples.

■ ABBREVIATIONS

AMPc, cyclic adenosine monophosphate; AU, arbitrary units; BSA, bovine serum albumin; CC_{50}, half cytotoxic concentration; CLZ, cilostazol; CuAAC, copper-assisted azide-alkyne cycloaddition; CuFAAC, copper-free assisted azide-alkyne cycloaddition; DLS, dynamic light scattering; DMEM, Dulbecco's modified Eagle's medium; DSC, differential scanning calorimetry; EE, encapsulation efficiency; FTIR-ATR, Fourier transformed infrared spectroscopy attenuated total reflectance; HIUS, high-intensity ultrasound; LPS, lipopolysaccharide; MMP, matrix metalloproteinase; MTT, 3-(4,5-dimethyl-2-thiazolyl)-2,5-diphenyl-2*H*-tetrazolium; MWCO, molecular weight cut off; NPs, nanoparticles; NRK, normal rat kidney; PAT, poly(amide-triazole); PET, poly-(ester-triazole); PAT-P-v, empty PAT nanoparticles with PVA as the stabilizer; PET-P-v, empty PET nanoparticles with PVA as the stabilizer; PAT-P-CLZ, CLZ-loaded PAT nanoparticles with PVA as the stabilizer; PET-P-CLZ, CLZ-loaded PET nanoparticles with PVA as the stabilizer; PBS, phosphate-buffered saline; PhM, physical mixture; PVA, poly(vinyl alcohol); r.t., room temperature; SDS, sodium dodecyl sulfate; SEM, scanning electron microscopy; T_g, glass-transition temperature

■ REFERENCES

(1) Galbis, J. A. A.; García-Martín, M. G.Sugars as Monomers. In *Monomers, Polymers and Composites from Renewable Resources*; Elsevier, 2008; Chapter 5, pp 89−114.

(2) Rivas, M. V.; Petroselli, G.; Erra-Balsells, R.; Varela, O.; Kolender, A. A. Synthesis, Characterization and Chemical Degradation of Poly(Ester-Triazole)s Derived from d-Galactose. *RSC Adv.* **2019**, *9*, 9860−9869.

(3) Rivas, M. V.; Varela, O.; Kolender, A. A. Galactose-Derived Poly(Amide-Triazole)s. Degradation, Deprotection and Derivatization Studies. *Eur. Polym. J.* **2020**, *130*, No. 109653.

(4) Fidalgo, D. M.; Kolender, A. A.; Varela, O. Poly(Amide-Triazole)s Obtained by Regioselective, Microwave-Assisted Click Polymerization of Bio-Based Monomers. *Mater. Today Commun.* **2015**, *2*, e70−e83.

(5) Biomaterials. *NATIONAL Inst. Biomed. IMAGING Bioeng. (NIBIB)*2019, No. December.

(6) Egle, R.; Milek, M.; Mlinarič-Raščan, I.; Fahr, A.; Kristl, J. A Novel Gene Delivery System for Stable Transfection of Thiopurine-S-Methyltransferase Gene in Versatile Cell Types. *Eur. J. Pharm. Biopharm.* **2008**, *69*, 23−30.

(7) Prabhu, R. H.; Patravale, V. B.; Joshi, M. D. Polymeric Nanoparticles for Targeted Treatment in Oncology: Current Insights. *Int. J. Nanomed.* **2015**, *10*, 1001−1018.

(8) Niaounakis, M.Introduction. In *Introduction Biopolymers: Processing and Products*; Elsevier, 2015; Chapter 1, pp 1−77.

(9) Daraba, O. M.; Cadinoiu, A. N.; Rata, D. M.; Atanase, L. I.; Vochita, G. Antitumoral Drug-Loaded Biocompatible Polymeric Nanoparticles Obtained by Non-Aqueous Emulsion Polymerization. *Polymers* **2020**, *12*, No. 1018.

(10) Iurciuc, C. E.; Atanase, L. I.; Jérôme, C.; Sol, V.; Martin, P.; Popa, M.; Ochiuz, L. Polysaccharides-based Complex Particles' Protective Role on the Stability and Bioactivity of Immobilized Curcumin. *Int. J. Mol. Sci.* **2021**, *22*, No. 3075.

(11) Grabnar, P. A.; Kristl, J. The Manufacturing Techniques of Drug-Loaded Polymeric Nanoparticles from Preformed Polymers. *J. Microencapsulation* **2011**, *28*, 323−335.

(12) des Rieux, A.; Fievez, V.; Garinot, M.; Schneider, Y. J.; Préat, V. Nanoparticles as Potential Oral Delivery Systems of Proteins and Vaccines: A Mechanistic Approach. *J. Controlled Release* **2006**, *116*, 1−27.

(13) Galindo-Rodriguez, S.; Allémann, E.; Fessi, H.; Doelker, E. Physicochemical Parameters Associated with Nanoparticle Formation in the Salting-out, Emulsification-Diffusion, and Nanoprecipitation Methods. *Pharm. Res.* **2004**, *21*, 1428−1439.

(14) Aryal, S.; Park, H.; Leary, J. F.; Key, J. Top-down Fabrication-Based Nano/Microparticles for Molecular Imaging and Drug Delivery. *Int. J. Nanomed.* **2019**, *14*, 6631−6644.

(15) Moghimi, S. M.; Hunter, A. C.; Murray, J. C. Nanomedicine: Current Status and Future Prospects. *FASEB J.* **2005**, *19*, 311−330.

(16) Molina-Pinilla, I.; Hakkou, K.; Romero-Azogil, L.; Benito, E.; García-Martín, M. G.; Bueno-Martínez, M. Synthesis of Degradable Linear Cationic Poly(Amide Triazole)s with DNA-Condensation Capability. *Eur. Polym. J.* **2019**, *113*, 36−46.

(17) Romero-Azogil, L.; Benito, J. M.; Pinilla, I. M.; Hakkou, K.; Martínez, M. B.; Cantón, I.; López-Cornejo, P.; García-Calderón, C. B.; Rosado, I. V.; García-Martín, M. G.; Benito, E. Structure-Property Relationships of D-Mannitol-Based Cationic Poly(Amide Triazoles) and Their Self-Assembling Complexes with DNA. *Eur. Polym. J.* **2020**, *123*, No. 109458.

(18) Ota, H.; Eto, M.; Kano, M. R.; Ogawa, S.; Iijima, K.; Akishita, M.; Ouchi, Y. Cilostazol Inhibits Oxidative Stress-Induced Premature Senescence via Upregulation of Sirt1 in Human Endothelial Cells. *Arterioscler., Thromb., Vasc. Biol.* **2008**, *28*, 1634−1639.

(19) Hiatt, W. R.; Money, S. R.; Brass, E. P. Long-Term Safety of Cilostazol in Patients with Peripheral Artery Disease: The CASTLE Study (Cilostazol: A Study in Long-Term Effects). *J. Vasc. Surg.* **2008**, *47*, 330−336.e2.

(20) Pu, X.; Sun, J.; Li, M.; He, Z. Formulation of Nanosuspensions as a New Approach for the Delivery of Poorly Soluble Drugs. *Curr. Nanosci.* **2009**, *5*, 417−427.

(21) Gomes, M. L. S.; da Silva Nascimento, N.; Borsato, D. M.; Pretes, A. P.; Nadal, J. M.; Novatski, A.; Gomes, R. Z.; Fernandes, D.; Farago, P. V.; Zanin, S. M. W. Long-Lasting Anti-Platelet Activity of Cilostazol from Poly(ε-Caprolactone)-Poly(Ethylene Glycol) Blend Nanocapsules. *Mater. Sci. Eng., C* **2019**, *94*, 694−702.

(22) Navarra, G.; Leone, M.; Militello, V. Thermal Aggregation of β-Lactoglobulin in Presence of Metal Ions. *Biophys. Chem.* **2007**, *131*, 52−61.
(23) Gomes, M. L. S.; Klein, T.; Simionatto, M.; Nadal, J. M.; Zanin, S. M. W.; Borsato, D. M.; Farago, P. V. A Simple RP-HPLC/UV Method for Determination of Cilostazol in Polymeric Nanoparticles Suspensions: Development and Validation. *Lat. Am. J. Pharm.* **2015**, *34*, 803−809.
(24) D'Souza, S. A Review of In Vitro Drug Release Test Methods for Nano-Sized Dosage Forms. *Adv. Pharm.* **2014**, *2014*, 1−12.
(25) Musikant, D.; Higa, R.; Rodríguez, C. E.; Edreira, M. M.; Campetella, O.; Jawerbaum, A.; Leguizamón, M. S. Sialic Acid Removal by Trans-Sialidase Modulates MMP-2 Activity during Trypanosoma Cruzi Infection. *Biochimie* **2021**, *186*, 82−93.
(26) Hassan, C. M.; Peppas, N. A.Structure and Applications of Poly (Vinyl Alcohol) Hydrogels Produced by Conventional Crosslinking or by Freezing/Thawing Methods. In *Biopolymers · PVA Hydrogels, Anionic Polymerisation Nanocomposites*; Springer Nature: Switzerland AG, 2000; Vol. *153*, pp 37−65.
(27) Junyapraset, V. B.; Boonme, P.; Songkro, S.; Krauel, K.; Rades, T. Transdermal Delivery of Hydrophobic and Hydrophilic Local Anesthetics from o / w and w / o Brij. *J. Pharm. Sci.* **2007**, *10*, 288−298.
(28) Eitel, K.; Bryant, G.; Schöpe, H. J. A Hitchhiker's Guide to Particle Sizing Techniques. *Langmuir* **2020**, *36*, 10307−10320.
(29) Berne, B. J.; Pecora, R.*Dynamic Light Scattering (With Applications to Chemistry, Biology, and Physics)*; Dover Publications, 2000.
(30) Merkus, H. G.*Particle Size Measurements: Fundamentals, Practice, Quality*; Springer, 2009.
(31) Kim, A.; Ng, W. B.; Bernt, W.; Cho, N. J. Validation of Size Estimation of Nanoparticle Tracking Analysis on Polydisperse Macromolecule Assembly. *Sci. Rep.* **2019**, *9*, No. 2639.
(32) Wilson, B. K.; Prud'homme, R. K. Nanoparticle Size Distribution Quantification from Transmission Electron Microscopy (TEM) of Ruthenium Tetroxide Stained Polymeric Nanoparticles. *J. Colloid Interface Sci.* **2021**, *604*, 208−220.
(33) Pazik, A.; Skwierawska, A. Synthesis and Spectroscopic Properties of New Bis-Tetrazoles. *J. Inclusion Phenom. Macrocyclic Chem.* **2013**, *77*, 83−94.
(34) Ghodsinia, S. S. E.; Akhlaghinia, B. A Rapid Metal Free Synthesis of 5-Substituted-1H-Tetrazoles Using Cuttlebone as a Natural High Effective and Low Cost Heterogeneous Catalyst. *RSC Adv.* **2015**, *5*, 49849−49860.
(35) Mansur, H. S.; Sadahira, C. M.; Souza, A. N.; Mansur, A. A. P. FTIR Spectroscopy Characterization of Poly (Vinyl Alcohol) Hydrogel with Different Hydrolysis Degree and Chemically Crosslinked with Glutaraldehyde. *Mater. Sci. Eng., C* **2008**, *28*, 539−548.
(36) Hdidar, M.; Chouikhi, S.; Fattoum, A.; Arous, M. Effect of Hydrolysis Degree and Mass Molecular Weight on the Structure and Properties of PVA Films. *Ionics* **2017**, *23*, 3125−3135.
(37) Bhattacharjee, S. DLS and Zeta Potential - What They Are and What They Are Not? *J. Controlled Release* **2016**, *235*, 337−351.
(38) Sternlicht, M. D.; Werb, Z. How Matrix Metalloproteinases Regulate Cell Behavior. *Annu. Rev. Cell Dev. Biol.* **2001**, *17*, 463−516.
(39) Tsai, C. S.; Lin, F. Y.; Chen, Y. H.; Yang, T. L.; Wang, H. J.; Huang, G. S.; Lin, C. Y.; Tsai, Y. T.; Lin, S. J.; Li, C. Y. Cilostazol Attenuates MCP-1 and MMP-9 Expression in Vivo in LPS-Administrated Balloon-Injured Rabbit Aorta and in Vitro in LPS-Treated Monocytic THP-1 Cells. *J. Cell. Biochem.* **2008**, *103*, 54−66.
(40) Umebayashi, R.; Uchida, H. A.; Kakio, Y.; Subramanian, V.; Daugherty, A.; Wada, J. Cilostazol Attenuates Angiotensin II-Induced Abdominal Aortic Aneurysms but Not Atherosclerosis in Apolipoprotein E-Deficient Mice. *Arterioscler., Thromb., Vasc. Biol.* **2018**, *38*, 903−912.
(41) Carvalho da Silva, F.; do Carmo Cardoso, M. F.; Garcia Ferreira, P.; Ferreira, V. F.Biological Properties of 1H-1,2,3- and 2H-1,2,3-Triazoles. In *Chemistry of 1,2,3-Triazoles*; Bakulev, W.; Dehaen, V. A., Eds.; Springer, 2014; pp 117−165.
(42) Avérous, L.; Pollet, E.Environmental Silicate Nano-Biocomposites. In *Green Energy and Technology*; Springer, 2012; Vol. *50*, pp 13−39.
(43) Pifferi, C.; Fuentes, R. F.; Fernández-Tejada, A. Natural and Synthetic Carbohydratebased Vaccine Adjuvants and Their Mechanisms of Action. *Nat. Rev. Chem.* **2021**, *5*, 197−216.
(44) Wang, L.; Bharti; Kumar, R.; Pavlov, P. F.; Winblad, B. Small Molecule Therapeutics for Tauopathy in Alzheimer's Disease: Walking on the Path of Most Resistance. *Eur. J. Med. Chem.* **2021**, *209*, No. 112915.
(45) Lee, Y. J.; Shu, M. S.; Kim, J. Y.; Kim, Y. H.; Sim, K. H.; Sung, W. J.; Eun, J. R. Cilostazol Protects Hepatocytes against Alcohol-Induced Apoptosis via Activation of AMPK Pathway. *PLoS One* **2019**, *14*, No. e0211415.
(46) Nagai, N.; Yoshioka, C.; Ito, Y.; Funakami, Y.; Nishikawa, H.; Kawabata, A. Intravenous Administration of Cilostazol Nanoparticles Ameliorates Acute Ischemic Stroke in a Cerebral Ischemia/Reperfusion-Induced Injury Model. *Int. J. Mol. Sci.* **2015**, *16*, 29329−29344.

https://doi.org/10.1021/acsomega.2c02969
ACS Omega 2022, 7, 44631−44642